Intrinsic dielectric and spectroscopic behavior of perovskite Ba (Ni 1 ⁄ 3 Nb 2 ⁄ 3) O 3 – Ba (Zn 1 ⁄ 3 Nb 2 ⁄ 3) O 3 microwave dielectric ceramics

I. N. Lin, C. T. Chia, H. L. Liu, H. F. Cheng, R. Freer, M. Barwick, and F. Azough

Citation: Journal of Applied Physics **102**, 044112 (2007); doi: 10.1063/1.2770870
View online: http://dx.doi.org/10.1063/1.2770870
View Table of Contents: http://scitation.aip.org/content/aip/journal/jap/102/4?ver=pdfcov
Published by the AIP Publishing

Intrinsic dielectric and spectroscopic behavior of perovskite $Ba(Ni_{1/3}Nb_{2/3})O_3-Ba(Zn_{1/3}Nb_{2/3})O_3$ microwave dielectric ceramics

I. N. Lin
Department of Physics, Tamkang University, Taipei, Taiwan 251

C. T. Chia, H. L. Liu, and H. F. Cheng
Department of Physics, National Taiwan Normal University, Taipei, Taiwan 117

R. Freer,[a] M. Barwick, and F. Azough
Materials Science Centre, School of Materials, University of Manchester, Grosvenor Street, Manchester, M1 7HS, United Kingdom

(Received 15 May 2007; accepted 13 July 2007; published online 24 August 2007)

Ceramics of $0.35Ba(Ni_{1/3}Nb_{2/3})O_3-0.65Ba(Zn_{1/3}Nb_{2/3})O_3$ were prepared by the mixed oxide route. The effect of the cooling rate (2 °C–240 °C/h) after sintering on the microwave dielectric properties of the ceramics was examined. While the extrinsic factors, such as porosity and secondary phases, markedly influence the dielectric properties in the low-frequency regime, they have minimal effect on these properties in the high-frequency regime. The mechanisms involved in modifying the high-frequency dielectric properties of the materials were investigated by Fourier transform infrared and Raman spectroscopy, in conjunction with the Rietveld analysis of x-ray diffraction (XRD) spectra. A reduction in the cooling rate after sintering results in an increase in the high-frequency $Q\times f$ (product of dielectric Q value and measurement frequency) from 42 to 58 THz in the high-frequency regime (~1.5 THz). Such behavior correlates very well with the increase in the B-site occupancy by Nb (deduced from the Rietveld analyses of XRD spectra) and the increase in the coherency of the lattice vibration (deduced from the reduction in the full-width-at-half-maximum of the $A_{1g}(O)$ Raman mode). In contrast, the cooling rate after sintering has very limited effect on the relative permittivity (varying from 40.8 to 41.9 at 1.5 THz), which is in accord with the phenomenon that the cell volume and the Raman shift of $A_{1g}(O)$ Raman mode are essentially independent of the cooling rate. © *2007 American Institute of Physics*.
[DOI: 10.1063/1.2770870]

I. INTRODUCTION

Complex perovskites with general formula $A(B_{1/3}B'_{2/3})O_3$, where $A=Ba^{2+}$, $B=Mg^{2+}$, Zn^{2+}, or Ni^{2+}, $B'=Ta^{5+}$ or Nb^{5+} show interesting and commercially important properties at microwave frequencies. These ceramics typically have high relative permittivity ε' (or dielectric constant K), low dielectric loss ε'' (also described in terms of high dielectric Q value), and small temperature coefficient of resonance frequency (τ_f).[1–5] These materials are commonly used as resonators in microwave devices and systems, particularly for communications applications. A high dielectric Q-factor combined with small or preferably zero τ_f is critical for such applications.

The dielectric losses in microwave dielectrics originate either intrinsically or extrinsically. The extrinsic losses are related to defects (vacancies, impurities), porosity or second phases, and chemical inhomogeneity, etc., which are heavily dependent on processing conditions, whereas the intrinsic losses are related to the material composition, crystal structure, and structural disorder, which are independent of processing conditions. Investigations of dielectric properties at microwave frequencies are sometimes controversial, because of the interference of extrinsic factors on dielectric loss. The most promising approach to understanding the intrinsic microwave dielectric properties of materials is to investigate their high-frequency response, including that in the submillimeter and infrared regimes, since the intrinsic losses are overwhelmingly stronger than the extrinsic losses[6–9] in the far-infrared region and beyond.

A number of dielectric ceramics have been investigated in the submillimeter and infrared ranges by backward-wave-oscillator (BWO) and Fourier transform infrared (FTIR) spectroscopy.[10,11] Coherent terahertz (THz) time-domain spectroscopy has also been applied to characterize the dielectric properties of a range of materials[12–14] in the millimeter and submillimeter wave regimes. Spectroscopic measurements of the complex perovskites $xBa(Mg_{1/3}Ta_{2/3})O_3-(1-x)Ba(Mg_{1/3}Nb_{2/3})O_3$ were performed in an attempt to understand the nature of these low-loss dielectric materials in terms of the lattice vibrational modes in the infrared region of the spectra.[15–17] Moreover, Raman spectroscopy provides valuable insight into order-disorder phenomena.[18–20] Raman scattering is very sensitive to sample composition and structural variations, making it suitable for studying the effects of atomic substitution on both the Raman phonon position as well as linewidth. In this way correlations between phonon vibrations and the microwave spectra can be addressed.

Today a wide variety of dielectric ceramics is available

[a]Author to whom correspondence should be addressed; FAX: +44-161-306-8877; electronic mail: robert.freer@manchester.ac.uk

for communications applications. For example, the perovskite ceramics $Ba(Zn_{1/3}Nb_{2/3})O_3$ (BZN) and $Ba(Ni_{1/3}Nb_{2/3})O_3$ (BNN) exhibit similar relative permittivities (~40 and 29, respectively), but τ_f values of opposite polarity. When BZN and BNN are combined in 0.65:0.35 ratio (i.e., $0.35Ba(Ni_{1/3}Nb_{2/3})O_3-0.65Ba(Zn_{1/3}Nb_{2/3})O_3$), a temperature-stable product is achieved, with τ_f ~0 ppm/°C, although the dielectric losses vary significantly with processing conditions.[21]

In this study, ceramics of $0.35Ba(Ni_{1/3}Nb_{2/3})O_3-0.65Ba(Zn_{1/3}Nb_{2/3})O_3$ have been investigated by Raman spectroscopy and FTIR spectroscopy, in an attempt to understand the relationship between the lattice vibrational modes and the intrinsic high-frequency dielectric properties of the materials.

II. EXPERIMENTAL DESCRIPTION

The $0.35Ba(Ni_{1/3}Nb_{2/3})O_3-0.65Ba(Zn_{1/3}Nb_{2/3})O_3$ ceramic samples, which are abbreviated as 35BNN-65BZN, were prepared by the conventional mixed oxide process. The starting materials were high-purity oxides $BaCO_3$, NiO, ZnO, and Nb_2O_5. These were mixed in appropriate proportions and vibro-milled with propan-2-ol and zirconia media for 24 h. After drying, the powders were calcined at 1100 °C–1200 °C for 4 h, then remilled and dried. Pellets of 20 mm diameter were uniaxially pressed at 100 MPa. For sintering, the pellets were surrounded by powder of the same composition, placed on an alumina plate and covered by alumina housing. Sintering was performed in a Vecstar VF1 chamber furnace at 1450 °C for 4 h. The standard heating rate was 240 °C h^{-1}; cooling rates were 240, 10, and 2 °C h^{-1}. Fired densities were determined by the Archimedes method. The relative permittivity and dielectric Q values were determined at 6 GHz by the Hakki-Coleman (parallel plate) method[22] in association with an HP 8720ET network analyzer. The temperature coefficient of resonant frequency (τ_f) was determined using a silver-plated aluminum cavity and network analyzer over the temperature range −10 °C–60 °C.

For microstructure analysis, sintered products were ground on SiC down to 1200 grade then polished with 6 μm and 1 μm diamond paste. A brief thermal etch at 1100 °C was sufficient to reveal the microstructure. The samples were examined using a Phillips XL30 FEG scanning electron microscope equipped with energy dispersive spectrometry (EDS). For x-ray diffraction analysis, polished and as-sintered samples were examined by a Philips PW1877, with Cu $K_{\alpha 1}$ radiation. Samples were scanned from $2\theta=10°$ to 110° in a continuous mode at 0.008° 2θ s^{-1}. The degree of ordering was initially determined from the ratio of the (100) hexagonal peak to the (110, 012, 102) peak. More detailed x-ray diffraction studies were undertaken using a synchrotron radiation x-ray source (beamline BL17C, National Synchrotron Radiation Research Center of Taiwan) from $2\theta=10°$ to 110°. Rietveld refinement yielded lattice parameters and occupancies of the major cation sites.

For FTIR spectroscopy, near-normal infrared reflectance spectra were collected at room temperature from polished surfaces. A Bruker IFS 66v Fourier transform infrared spectrometer was used in the far-infrared and mid-infrared regions (40–4000 cm^{-1}). The modulated light beam from the spectrometer was focused onto either the sample or a gold reference mirror, and the reflected beam was directed onto a 4.2 K bolometer detector (40–600 cm^{-1}) and a B-doped Si photoconductor (450–4000 cm^{-1}). The different sources, beam splitters, and detectors used in these studies provided substantial spectral overlap, and the reflectance mismatch between adjacent spectral ranges was less than 1%. The optical properties, i.e., the complex conductivity $\sigma(\omega)=\sigma_1(\omega)+i\sigma_2(\omega)$ or dielectric function $\varepsilon(\omega)=1+4\pi i\sigma(\omega)/\omega$, were calculated from Kramers-Kronig analysis of the reflectance data.[15] To perform these transformations it is necessary to extrapolate the reflectance data to both low and high frequencies. The extension was achieved by modeling the reflectance with the Lorentz model and using the fitted results to extend the reflectance below the lowest frequency measured in the experiment. The high-frequency extrapolations were performed by employing a weak power-law dependence, $R \sim \omega^{-s}$, with $s \sim 1-2$.

A DILOR XY 800 triple-grating Raman spectrometer equipped with a liquid-nitrogen-cooled charge-coupled device (CCD) was used for micro-Raman measurements. The 514.5 nm line of an Ar^+ ion laser with 10 mW output was used as the excitation source and an Olympus BH-2 microscope with 100× objective was employed for room-temperature micro-Raman detection. The recorded Raman spectra had a resolution of approximately 1 cm^{-1}.

III. RESULTS AND DISCUSSION

The sintered density of the ceramics increased from 93% to 98% theoretical as cooling rate decreased, reflecting the increased time that the specimens spent at elevated temperature. Laboratory-based x-ray diffraction analysis of ground surfaces revealed a single-phase, cubic structure ($Pm3m$) for rapidly cooled (240 °C/h) samples [Fig. 1(a)], containing no ordering peaks, but a pseudocubic structure ($P\bar{3}m1$, hexagonal) for slowly cooled (i.e., 10° and 2 °C/h) samples [Fig. 1(b)], with clear evidence of ordering. It should be noted that the ions in the 240 °C/h-cooled samples are possibly also ordered, but the degree of ordering is too weak to be resolved by conventional x-ray diffractometry. A more sophisticated technique is required to elucidate such a phenomenon; this will be discussed later.

Figure 2 shows a typical micrograph of the polished surface of a $0.35Ba(Ni_{1/3}Nb_{2/3})O_3-0.65Ba(Zn_{1/3}Nb_{2/3})O_3$ ceramic. While the bulk of the ceramic is the $0.35Ba(Ni_{1/3}Nb_{2/3})O_3-0.65Ba(Zn_{1/3}Nb_{2/3})O_3$ phase (region *A*), the outer rim comprises two Zn-deficient phases $Ba_8(ZnNb_6)O_{24}$ (region *B*) and $Ba_5Nb_4O_{15}$ (region *C*).[23] The samples cooled at 2 °C/h exhibited near-chemical homogeneity within matrix grains and large grains (~2.8 μm). In contrast, the rapidly cooled (240 °C/h) samples exhibited two distinct compositions: BNN grains containing low levels of Zn, and BZN grains containing low levels of Ni, both relatively small in size (~0.8 μm). Thus, sintering at 1450 °C for 4 h followed by rapid cooling was sufficient to

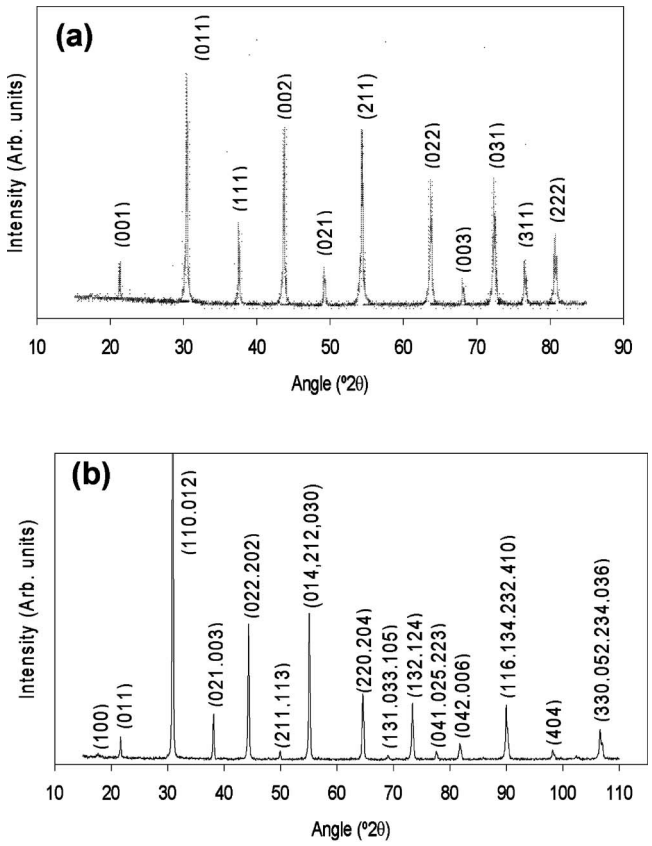

FIG. 1. X-ray diffraction spectra of 0.35BNN-0.65BZN ceramic sintered at 1450 °C for 4 h.(a) cooled at 240 °C h^{-1} (structure $Pm3m$); (b) cooled at 2 °C hr^{-1} (structure P-$3m1$).

develop dense materials, with relatively uniform microstructure, but insufficient to achieve chemical homogeneity. Table I summarizes the materials' characteristics and dielectric properties of the ceramics at 6 GHz. While there is little change in relative permittivity (36.0 to 33.2), there are significant changes in dielectric Q values, with $Q\times f$ increasing from 1673 to 16 208 GHz as cooling rate after sintering decreased from 240 °C/h to 2 °C/h. Thus, as samples are cooled more slowly there is an increase in sample homogeneity, grain size, and the degree of ordering and, therefore, a significant improvement in quality factor at 6 GHz. The dielectric Q value is generally more sensitive to minor changes in composition and processing conditions than relative permittivity.

Clearly, the modifications to dielectric properties in response to changes in processing conditions depend on both extrinsic and intrinsic factors. The observations described above demonstrate the effect of extrinsic factors, particularly

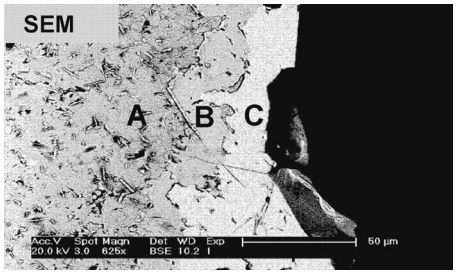

FIG. 2. SEM micrograph of the polished surface of 0.35BNN-0.65BZN ceramic cooled at 2 °C hr^{-1}, showing 35/65 phase in the core region (a), $Ba_8(ZnNb_6)O_{24}$-type phase (b), and $Ba_5Nb_4O_{15}$ phase (c).

porosity and inhomogeneity, on the dielectric properties of the BNN-BZN materials in the microwave frequency regime. However, it is not clear how the materials' characteristics affect the dielectric properties of BNN-BZN and related materials in the terahertz frequency regime, which is of relevance to future telecommunication systems. FTIR spectroscopy was used to explore the higher frequency dielectric properties, as it can effectively probe and evaluate the terahertz dielectric properties.

Figure 3(a) shows the frequency dependence of the reflection coefficient obtained from FTIR spectroscopy. These data were transformed into conductivity-frequency (σ_1–f) spectra [Fig. 3(b)] via the Kramers-Kronig relationship[15] to reveal the contribution of lattice vibrational modes to the microwave dielectric properties of the materials. Figure 3(b) shows the contribution of phonons in the small wave number (10–1000 cm^{-1}) regime and that of electronic interband transitions in the large wave number (>1000 cm^{-1}) regime to the dielectric response of the materials. The real part (ε_1) and imaginary part (ε_2), of relative permittivity, and the quality factor ($Q=\varepsilon_1/\varepsilon_2$) can also be extracted from the frequency dependence of reflectance data by using the Lorentz model, Eqs. (1) and (2),

$$\varepsilon_1 = \varepsilon_\infty + \sum_j \left(\frac{4\pi e^2 N_j}{mV}\right)\frac{1}{\omega_{0j}^2} = \varepsilon_\infty + \sum_j 4\pi\rho j, \tag{1}$$

$$\frac{1}{Q} = \sum_j \tan\,\delta_j = \sum_i \frac{4\pi\rho_j\gamma_j\omega}{\omega_{0j}^2\varepsilon_1}, \tag{2}$$

where resonance frequency (ω_{0j}), the damping coefficient (γ_j), and the resonance strength ($4\pi\rho_j$) of the jth mode resonator are dispersion parameters for the lattice vibration,[15–17] which can be extracted from the reflectance spectra shown in Fig. 3(a). These dispersion parameters are the most important parameters used for estimating the real and imaginary part of

TABLE I. Physical and dielectric properties of $0.35Ba(Ni_{1/3}Nb_{2/3})O_3$–$0.65Ba(Zn_{1/3}Nb_{2/3})O_3$ ceramics at microwave (6 GHz) and THz frequencies (1.0–1.5 THz—obtained by FTIR spectroscopy).

Cooling rate (°C/h)	Density (% theoretical)	Grain size (μm)	Microwave ε_r (6 GHz)	Microwave $Q\times f$ (6 GHz)	FTIR ε_r (1.5 THz)	FTIR $Q\times f$ (1.5 THz)
240	92.9	0.8	36.0	1673	41.9	42
10	95.4	1.7	33.8	9585	41.2	49
2	98.1	2.8	33.2	16208	40.8	58

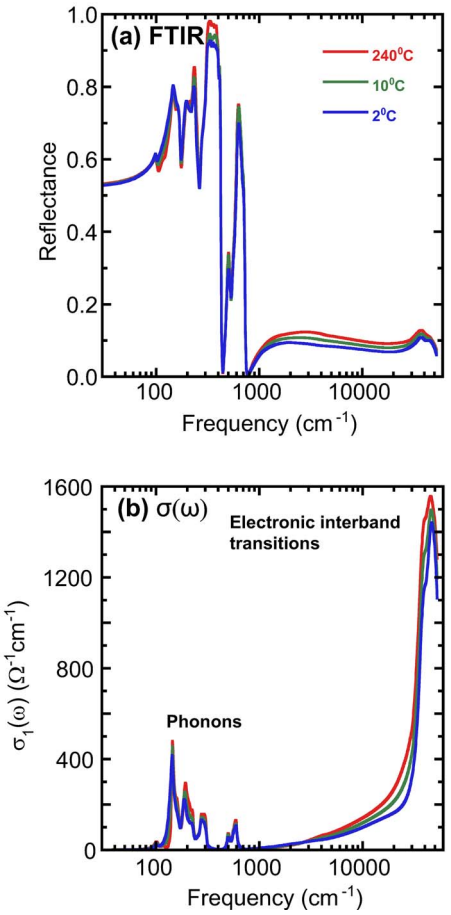

FIG. 3. (Color online) (a) Reflectance-frequency data obtained by FTIR spectroscopy, and (b) conductivity- frequency properties derived from the reflectance-frequency data using the Kramer-Kronig relationship, for 0.35BNN-0.65BZN ceramics sintered at 1450 °C for 4 h and the cooled at 2–240 °C/h after sintering.

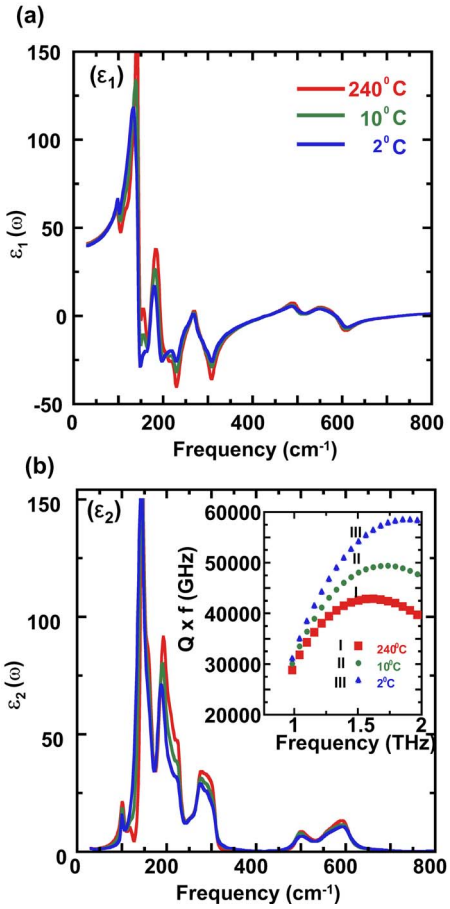

FIG. 4. (Color online) The (a) real part (ε_1) and (b) imaginary part (ε_2) of dielectric constant, derived from the reflectance-frequency data using Kramer-Kronig relationship, for the 0.35BNN-0.65BZN ceramics, which were sintered at 1450 °C for 4 h and cooled at 2–240 °C/h after sintering [the inset in (b) shows the high-frequency quality factor, $Q=\varepsilon_1/\varepsilon_2$, in the 1–2 THz regime, estimated from the dielectric data shown in this figure].

dielectric response. The frequency dependency of ε_1 and ε_2, which was deduced in this way, are presented in Figs. 4(a) and 4(b), respectively. It should be noted that all the vibrational modes contribute to the dielectric response of the materials. Therefore, in order to accurately estimate the dielectric response of the materials using FTIR spectroscopy, we need to include all the resonance modes, i.e., the measuring range in FTIR spectroscopy should be extended to a sufficiently low wave number. Fortunately, for the BNN-BZN materials, 40 cm^{-1} is adequate to excite all the possible FTIR resonance modes, as first-principles calculations have confirmed that the lowest FTIR mode is around 75 cm^{-1}.[24]

The terahertz quality factor data ($Q=1/\tan\delta=\varepsilon_1/\varepsilon_2$) in the 1–2 THz frequency regime evaluated from Figs. 4(a) and 4(b), are plotted in the inset of Fig. 4(b). It is interesting to note that, while the dielectric properties measured in the low-frequency regime (6 GHz) are very sensitive to the postsintering process (the cooling rate), the dielectric constant and quality factor of the materials measured in the high-frequency regime (~1 THz) are essentially the same ($\varepsilon_1=40$ and $Q\times f=30$ THz), regardless of the postsintering process. These results imply that the extrinsic factors no longer impose the same dominating effect on the dielectric properties of the materials in the terahertz frequency regime as that in the microwave frequency regime. Thus, while the extrinsic dielectric properties of the materials are extremely sensitive to the sample's processing conditions, the intrinsic dielectric properties of the materials estimated from FTIR are much less sensitive to such variations.

The intrinsic dielectric properties at 1.5 THz of the materials are presented in Table I. This shows that the intrinsic ε_1-values at 1.5 THz for the different materials are essentially the same [$(\varepsilon_1)_{1.5\ \mathrm{THz}}=40.8-41.9$], irrespective of cooling rate after sintering, whereas the intrinsic quality factor at 1.5 THz of the materials varies markedly with the postsintering processes [$(Q\times f)_{1.5\ \mathrm{THz}}=42.0-58.0$ THz]. The slower the cooling rate, the higher the terahertz $Q\times f$ values. Moreover, the $(Q\times f)_{1.5\ \mathrm{THz}}$-values determined at 1.5 THz are larger than those determined at 1.0 THz, the $(Q\times f)_{1.0\ \mathrm{THz}}$ values [inset, Fig. 4(b)], which is presumably due to the occurrence of a vibrational resonance mode near 100 cm^{-1}.

There is considerable evidence[16–18] that cation ordering in perovskites is accompanied by substantial improvement in the dielectric Q-value in the high-frequency regime. It is quite clear from the present study that there are subtle but important changes in the coherency of the lattice vibrations. Raman spectroscopy is a powerful technique that yields information and insight into mechanisms contributing to di-

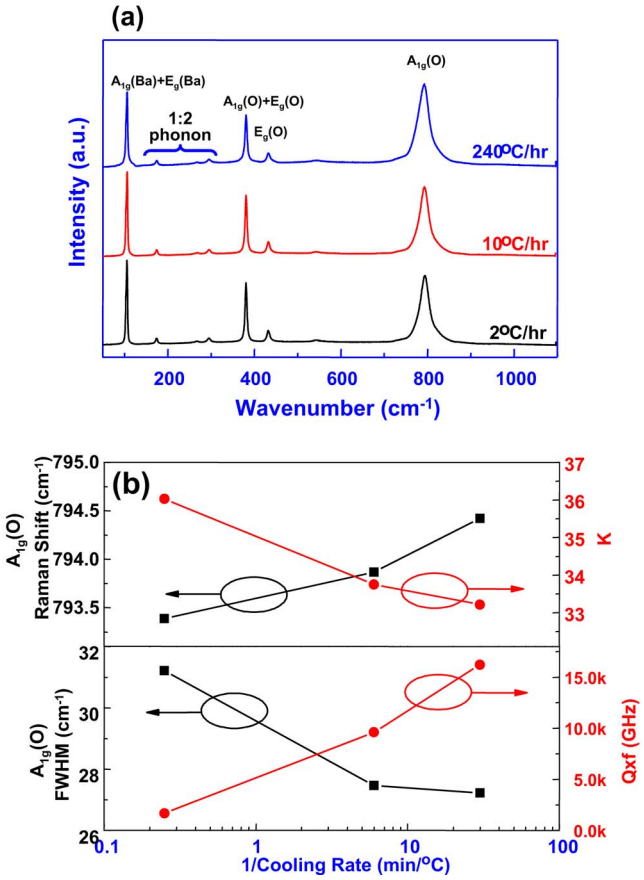

FIG. 5. (Color online) (a) Raman spectra, and (b) Raman shift and FWHM values for 0.35BNN-0.65BZN ceramics as a function of cooling rate after sintering. In (b), relative permittivity and $Q\times f$ data are included for comparison purposes; the characteristics are plotted against the inverse cooling rate $(1/r_c)$.

electric loss. Although the $Q\times f$ values for the slowly cooled products are not the highest recorded for $Ba(Ni_{1/3}Nb_{2/3})O_3-Ba(Zn_{1/3}Nb_{2/3})O_3$ ceramics,[21] the effect of ordering characteristics on the lattice vibrations and the effect of such differences on intrinsic dielectric properties can still be clearly resolved by these spectroscopic techniques.

To understand how the intrinsic dielectric properties of the materials vary with the cooling rate after sintering, the Raman spectra of these materials were examined. Figure 5(a) shows the Raman spectra for the 0.35BNN-0.65BZN ceramics. Since the structures of the materials and the spectra are very similar to those for the analogous BMT-BMN (Refs. 17 and 18) ceramics, the major peaks in the Raman spectra for BNN-BZN may be identified unambiguously. Most of the Raman resonance peaks [Fig. 5(a)] are very sharp, indicating that the lattice vibrations are quite coherent, an important factor for achieving high $Q\times f$ values in the materials. The presence of 1:2 order phonon peaks in the 160–300 cm^{-1} frequency regime indicates that the materials are highly ordered. It should be noted that the Raman spectra of not only the slowly cooled (2 °C/h) samples, but also the 240 °C/h-cooled ones exhibit ordered phonon peaks. These results indicate that Raman spectroscopy is much more sensitive to the ordering of ions than conventional laboratory-based x-ray diffractometry.

Previous Raman spectroscopy studies[17,18] of complex perovskites demonstrated that modification of the characteristics of the $A_{1g}(O)$ lattice vibration modes, which corresponds to the breathing modes of the NbO_6-octahedron cage, is the single most important factor reflecting the dielectric response of such materials. The variation of the shift and the FWHM (full-width at half-maximum) of the $A_{1g}(O)$ Raman peaks for the BNN-BZN samples as a function of cooling rate is detailed in Fig. 5(b), where the Raman characteristics are plotted against the inverse cooling rate, $(1/r_c)$. The Raman shift is very small for all the samples (f=793.4 −794.6 cm^{-1} and Δf=0–1.2 cm^{-1}). However, detailed analysis reveals that the Raman shift is slightly larger for the samples cooled at the slower rate (r_c), or larger $1/r_c$, which corresponds to the smaller relative permittivity, or K-value. The relative permittivity of the samples decreases with $1/r_c$ but at a very moderate rate. In contrast, the FWHM value decreases markedly with increasing $1/r_c$ value, which corresponds to the improvement in the sharpness of the $A_{1g}(O)$ Raman resonance mode in response to the decrease in cooling rate (increase in $1/r_c$) after sintering. This phenomenon corresponds to the improvement in the coherency of the lattice vibrations for the slowly cooled samples. Essentially, the slowly cooled samples possess higher vibrational coherency and thus exhibit a significantly higher quality factor ($Q\times f$), whereas the rapidly cooled samples possess poorer vibrational coherency and thus exhibit inferior $Q\times f$ values.

Nevertheless, why the cooling rate alters the lattice vibrational behavior of the materials is still not fully understood. We, thereafter, undertook a more detailed analysis of the crystal structure of the materials via a Rietveld analysis of the synchrotron x-ray diffraction (XRD) spectra of the BNN-BZN materials. Figure 6(a) shows the XRD spectra obtained using a rotating-anode-diffractometer; the XRD spectra appear to be essentially the same, regardless of the cooling rate that the samples experienced. In fact, a detailed crystallographic study of BNN-BZN ceramics by Cernik *et al.*[25] indicated that high-resolution x-ray diffraction spectra, for slowly cooled and rapidly cooled samples, could be deconvoluted to yield four components representing the ordered and disordered fractions of BZN and BNN in each; the ratios changed with cooling rate. Such detailed treatment is outside the scope of this study and we therefore concentrate on the occupancy of the B-site by Nb and the cell parameters/volume changes. In this analysis, the goodness of fit for the refined data was very similar, with χ^2 values being typically 2–3 (Table II). As the secondary phases comprised a rim approximately 40 μm wide on the surface of a sample typically 16 mm in diameter, no attempt was made to include the minor phases in any refinement. Rietveld analysis of the data shows that the Nb-ion occupancy of the B-sites increases as the cooling rate decreases [larger $1/r_c$; Table II and Fig. 6(b)]. The higher level of Nb-ion occupancy indicates that the B-site ions of the materials are better ordered. Figures 5(b) and 6(b) imply that improved ordering of the B-site cations results in greater coherency of the lattice vibrational modes, an important mechanism contributing to the higher quality factor ($Q\times f$) of the materials. Figure 6(b) also shows that the cell volume varies slowly with sample

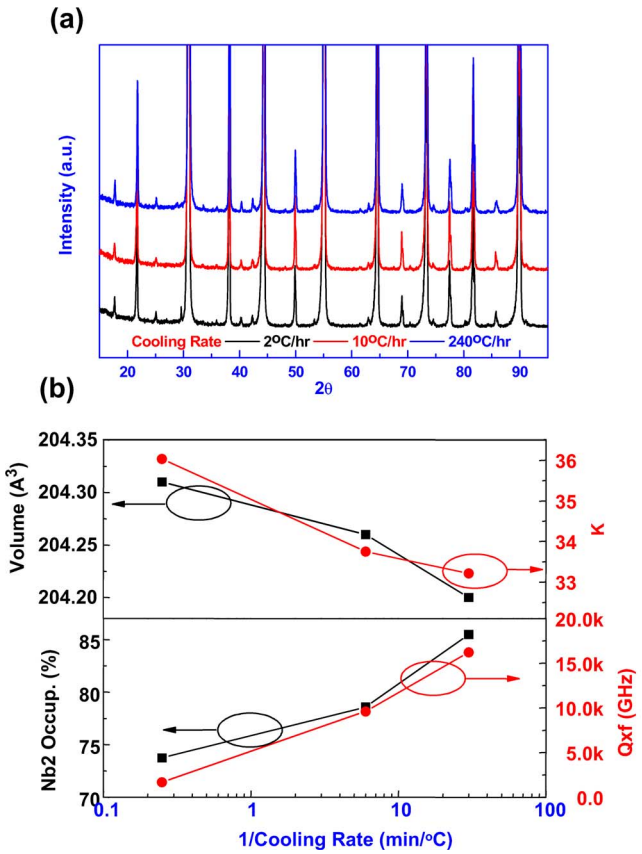

FIG. 6. (Color online) (a) X-ray diffraction spectra obtained by rotating-anode diffractometer and (b) the unit cell volume and Nb-ion site occupancy derived by Rietveld technique, for the 0.35BNN-0.65BZN ceramics sintered at 1450 °C for 4 h and then cooled at 2–240 °C/h after sintering [in (b), the characteristics were plotted against inverse of cooling rate, $1/r_c$].

cooling rate. The polarizability and hence the relative permittivity of the materials is thus comparatively insensitive to the processing parameters, which is in accord with the phenomenon that Raman shift of the $A_{1g}(O)$ peak is relatively insensitive to the processing parameters.

It should be remembered that, while the Raman spectroscopy yields a very strong correlation between the characteristics of the vibrational modes of the materials and their microwave dielectric response, the Raman resonance modes are nonpolar and cannot be directly correlated with the dielectric response of the materials. In contrast, the resonance modes in FTIR are in direct response to the polarization of materials with respect to an alternating field (infrared), and thus provide a more direct measurement of the dielectric properties of the materials. However, the FTIR spectra are extremely complicated and need sophisticated data processing techniques for full evaluation.

TABLE II. Lattice parameters, unit cell volume, occupancy of *B*-sites by Nb, and goodness of fit for Reitveld refinement of x-ray diffraction data for $0.35Ba(Ni_{1/3}Nb_{2/3})O_3-0.65Ba(Zn_{1/3}Nb_{2/3})O_3$ ceramics.

	$0.65Ba(Zn_{1/3}Nb_{2/3})O_3+0.35Ba(Ni_{1/3}Nb_{2/3})O_3$		
Cooling	2 °C/hr	10 °C/hr	240 °C/hr
a/b(Å)	5.7685	5.7707	5.7699
c(Å)	7.0860	7.0826	7.0863
Volume	204.20	204.26	204.31
K (ε_r)	33.2	33.8	36.0
Nb2-Occu.	85.47%	78.56%	73.74%
$Q\times f$ (GHz)	16208	9585	1673
χ^2	2.13	3.37	2.99

IV. CONCLUSIONS

The variation in the microwave dielectric properties of 0.35BNN-0.65BZN ceramics was examined as a function of cooling rate after sintering. While the extrinsic factors (porosity, inhomogeneity) dominate the dielectric properties in the low-frequency regime, they have very limited effect in the terahertz frequency regime. The intrinsic dielectric loss mechanisms are more closely related to lattice vibrations, which were investigated using FTIR and Raman spectroscopies, in conjunction with the Rietveld analysis of XRD spectra. A slower cooling rate resulted in enhanced $Q\times f$ values for the materials, but had comparatively little effect on the relative permittivity. This correlates very well with the increase in *B*-site occupancy, while the cell volume changed little as the cooling rate is decreased. These phenomena are consistent with the facts that, as the sample cools more slowly after sintering, the Raman shifts are changed insignificantly, whereas the FWHM of the Raman peaks decreases significantly.

ACKNOWLEDGMENTS

The authors gratefully acknowledge the financial support from the National Science Council of Taiwan, through Project No. NSC. 93-M2212-007-032, the Royal Society of Great Britain through award NC/Taiwan JP 04-06, and the provision of an EPSRC Doctoral Training Award (to M.B.).

[1] S. Nomura, K. Toyama, and K. Kaneta, Jpn. J. Appl. Phys., Part 1 **21**, 936 (1982).
[2] M. Onoda, J. Kuwata, K. Kaneta, K. Toyama, and S. Nomura, Jpn. J. Appl. Phys., Part 1 **21**, 1707 (1982).
[3] S. Nomura, Ferroelectrics **49**, 61 (1983).
[4] S. Nomura, T. Konoike, Y. Sakabe, and K. Wakino, J. Am. Ceram. Soc. **67**, 59 (1984).
[5] R. Guo, A. S. Shalla, and L. E. Cross, J. Appl. Phys. **75**, 4704 (1994).
[6] J. Petzelt, S. Pacesova, J. Fousek, S. Kamba, V. Zelezny, V. Koukal, J. Schwarzbach, B. P. Gorshunov, G. V. Kozlov, and A. A. Volkov, Ferroelectrics **93**, 77 (1989).
[7] G. O. Rupprecht and R. O. Bell, Phys. Rev. **125**, 1915 (1962).
[8] B. D. Silverman, Phys. Rev. **125**, 1921 (1962).
[9] V. L. Gurevich and A. K. Tagantsev, Adv. Phys. **40**, 719 (1991).
[10] J. Petzelt, R. Zurmuhlen, A. Bell, S. Kamba, G. V. Kozlov, A. A. Volkov, and N. Setter, Ferroelectrics **133**, 205 (1992).
[11] J. Petzelt, S. Kamba, G. V. Kozlov, and A. A. Volkov, Ferroelectrics **176**, 145 (1996).
[12] P. Kuzel and J. Petzelt, Ferroelectrics **239**, 949 (2000).
[13] T. R. Tsai, M. H. Liang, C. T. Hu, C. C. Chi and I. N. Lin, Jpn. J. Appl. Phys., Part 1 **39**, 5642 (2000).
[14] T. R. Tsai, M. H. Liang, C. T. Hu, C. C. Chi, and I. N. Lin, J. Eur. Ceram. Soc. **21**, 2787 (2001).
[15] F. Wooten, *Optical Properties of Solids* (Academic, New York, 1972).
[16] J. Petzelt, R. Zurmuhlen, A. Bell, S. Kamba, G. V. Kozlov, A. A. Volkov, and N. Setter, Ferroelectrics **133**, 205 (1992).
[17] Y. C. Chen, H. F. Cheng, H. L. Liu, C. T. Chia, and I. N. Lin, J. Appl. Phys. **94**, 3365 (2003).
[18] C. T. Chia, Y. C. Chen, H. F. Cheng, and I. N. Lin, J. Appl. Phys. **94**, 3360 (2003).
[19] I. G. Siny, R. W. Tao, R. S. Katiyar, R. A. Guo, and A. S. Bhalla, J. Phys. Chem. Solids **59**, 18 (1998).

[20]R. L. Moreira, F. M. Matinaga, and A. Dias, Appl. Phys. Lett. **78**, 428 (2001).
[21]M. Barwick, F. Azough, and R. Freer, J. Eur. Ceram. Soc. **26**, 1767 (2006).
[22]B. W. Hakki and P. D. Coleman, IEEE Trans. Microwave Theory Tech. **18**, 402 (1980).
[23]H. Hughes, F. Azough, and R. Freer, J. Eur. Ceram. Soc. **25**, 2755 (2005).
[24]H. C. Hsueh, S. L. Lee, W. C. Lee, H. L. Liu, C. T. Chia, and I. N. Lin (private communication).
[25]R. J. Cernik, M. Barwick, F. Azough, and R. Freer, J. Appl. Crystallogr. (in press).